Title: Energy saving potential of a hybrid HVAC system with a desiccant wheel activated at low temperatures and an indirect evaporative cooler in handling air in buildings with high latent loads

Authors: F. Comino*, M. Ruiz de Adana, F. Peci

Departamento de Química-Física y Termodinámica Aplicada, Escuela Politécnica Superior, Universidad de Córdoba, Campus de Rabanales, Antigua Carretera Nacional IV, km 396, 14071 Córdoba, España

*Corresponding author tel. +34 626285994; e-mail: francisco.comino@uco.es (F. Comino)

Abstract

Air handling in buildings with high latent loads usually requires a high-energy cost to satisfy the user's thermal comfort needs. Hybrid systems composed of desiccant wheels, DW, and indirect evaporative coolers, IEC, could be an alternative to direct expansion conventional systems, DX systems. The main objective of this work was to determine the annual energy consumption of a hybrid system with a DW activated at low temperatures and an IEC, DW-IEC system, compared to a DX system to serve air in a small building with high latent loads, such as spas. Several annual energy simulations for 6 climate zones were performed, analysing electric energy consumption, seasonal mean coefficient of performance, SCOP, and energy consumption per unit of dehumidified water, E_{cons}, of each system. The simulations were based on experimentally validated models.

The annual energy consumption of the DW-IEC system was lower than that of the DX system for the 6 climate zones, achieving significant energy savings, up to 46.8%. These energy savings resulted in better SCOP values for the DW-IEC system. Therefore, the proposed DW-IEC system has high potential to reduce energy costs, achieving the user's thermal comfort.

Keywords: hybrid system; desiccant wheel; indirect evaporative cooler; high latent loads; climate zones

Nomenclature

b	estimated parameter
C	capacity rate of air [kJ h^{-1} K^{-1}]
c_p	specific heat of air [kJ kg^{-1} K^{-1}]
CO	condenser
COP	coefficient of performance
DW	desiccant wheel
DX	direct expansion
EA	exhaust air
E_{cons}	energy consumption per unit of dehumidified water [Wh kg^{-1}]
EIR	electrical input ratio
EV	evaporator
IEC	indirect evaporative cooler
h	air specific enthalpy [kJ kg^{-1}]
HC	heating coil
k	number of parameters
MRC	moisture removal capacity [kg h^{-1}]
$\dot{m}$	mass air flow rate [kg h^{-1}]
$\dot{M}_{pool}$	evaporated water flow of the pool [kg h^{-1}]
Np	number of people
OA	outdoor air
PLF	partial load factor
P	static pressure [mmca]
$\dot{Q}$	heat transfer [kW]
RA	return air
S	area [m^2]
SCOP	seasonal mean coefficient of performance
SHE	sensible heat exchanger
T	dry bulb temperature [ºC]
T_{wb}	wet bulb temperature [ºC]
UA	overall heat transfer coefficient [kJ h^{-1} K^{-1}]
v	air velocity [m s^{-1}]
$\dot{V}$	volumetric air flow rate [m^3 h^{-1}]
$\dot{V}_w$	water flow rate of indirect evaporative cooler [l h^{-1}]
$\dot{W}$	electric power consumption [kW]
X	input variable
$\hat{Y}$	estimated output value

Greek letters

Δ	increase
ε	effectiveness
ρ	density [kg m^{-3}]
∑	sum
ω	humidity ratio [g kg^{-1}]
Ω	specific mass air flow rate [kg s^{-1} m^{-3}]

Subscripts

a	air
c	condenser
e	evaporator

HC	heating coil
i	inlet
IA	indoor air
lat	latent
N	nominal
o	outlet
OA	outdoor air
p	process air; primary air
s	secondary air
r	regeneration air
sen	sensible
t	total
T	temperature
w	water
Superscripts	
'	dimensionless value

1 Introduction

Air handling in buildings with high latent loads usually requires a high-energy cost to satisfy the user’s thermal comfort needs. Indoor swimming pools or spas are some examples of this type of buildings, which have high internal latent gains, due to the great amount of evaporated water from the wet areas [1]. Excessive air humidity can cause discomfort for the occupants and problems related to the indoor air quality of the building due to fungus and rot [2]. Therefore, an air handling system is required to control the indoor moisture content, while keeping a low energy consumption.

A traditional method of dehumidifying rooms with high latent loads is to introduce a certain air flow rate from outside, this method can only be used when the outdoor humidity ratio is lower than the indoor humidity. In this method [3], the air flow rate required to dehumidify the building was very high. The recommended air change rates per hour values were shown to vary between 4 h^{-1} and 7 h^{-1} in order to obtain thermal comfort [3]. This dehumidification method could cause discomfort to the occupants in small rooms with high latent loads, such as spas, due to the high air change rates per hour values.

Another method widely used in dehumidifying air is that of conventional dehumidification systems based on direct expansion units, DX system, which operates according to the vapor-compression cycle. DX systems reduce the air temperature below its dew point in order to condense water. An increase in the cooling power of the DX system usually produces an increase in its desiccant capacity. However, DX systems have a cooling capacity limit when the required dew-point temperature is very low, close to 0 °C, the freezing point of water. Moreover, the outlet air temperature of DX systems is usually very low, so a post-heating of air flow is necessary, before being supplied to the building. Several DX systems have been studied for indoor swimming pools [4,5], where high energy consumption values were required to dehumidify and heat the air steam. A comparative study between a DX system and an open absorption system to handle air in an indoor swimming pool, was carried out by other authors [6], obtaining significant energy savings with the open absorption system. These studies show the need to search for new HVAC systems in buildings with high latent loads.

Previous studies on energy saving in spas with small volumes and high latent loads have been carried out [7–9]. However, these works focused on the hot water system of swimming pools.

Desiccant dehumidification systems present an alternative solution to DX systems. Desiccant dehumidification systems adsorb water from the air in contact with an area of low vapour pressure at the surface of the desiccant [10]. One type of desiccant dehumidification system widely used is the desiccant wheel, DW, [11,12]. The most influential parameter on the desiccant capacity of a DW is the regeneration temperature [13,14]. Usually, DWs are thermally activated at high temperatures, from 60 ºC to 120 °C [15,16], although other studies also showed acceptable DW performance when their regeneration temperatures were below 60 °C [17]. The main disadvantage of DWs is the high outlet process air temperatures [18]. This heat is generated by the adsorption process of the DW, which is delivered from the regeneration section to the process section. Therefore, a cooling system is needed to lower the process air temperature before being supplied.

Cooling systems based on evaporators of a DX system are usually combined with a DW [19,20], but these systems normally require a high energy consumption [21]. Another cooling system that is usually combined with DWs is the evaporative cooler. There are two types: the direct evaporative cooler and the indirect evaporative cooler. The indirect evaporative cooler, IEC, system is one of the most promising technologies in reducing the air temperature because of its higher energy saving capacity compared to DX systems [22]. The IEC system requires two separate air flows to operate. The primary air flow which is cooled and supplied to the building without increasing its humidity ratio and the secondary air flow which is humidified with water supplied to the outside [23].

Many studies about IEC integrated into a desiccant system have been carried out [24–26]. An experimental study on a hybrid system composed of a DW and an IEC was carried out for several summer days in Italy [27]. This system reduced the electrical consumption significantly compared to one composed of a DW and two cooling coils fed by a conventional vapour compression chiller. A numerical simulation study on desiccant units presented a comparative analysis of three different systems with a DW and an IEC [28]. The results of this study indicated that all of them were able to obtain satisfactory supply air temperatures, even when the DW was regenerated at low temperature. Other numerical studies analysed the behaviour of a DW combined with an IEC system [29–32]. They were mainly based on the hybrid system performance optimization under different steady state air conditions, always using the IEC system to cool the output air stream of the DW.

Based on the limitations in the air treatment with conventional HVAC systems within the framework of air conditioning in buildings with small volume and high latent loads, such as spas, it would be interesting to analyse the energy saving potential and the annual behaviour of a novelty hybrid system based on DW and IEC in handling air in buildings with high latent loads and low supply air flow rates, decoupling sensible and latent loads by using low temperature energy sources. The main objective of this work was to determine the annual energy consumption of a hybrid HVAC system composed of a DW activated at low temperatures and an IEC, compared to a DX system composed of a direct expansion unit for a small building with high latent loads. Hence, several annual energy simulations for different climate zones were carried out. Electric energy consumption, $\dot{W}$, seasonal mean coefficient of performance, SCOP, and energy consumption per unit of dehumidified water, E_{cons}, of each system were analysed.

2 Methodology

2.1 System description

A criterion commonly used by manufacturers to select dehumidification units, is their moisture removal capacity, MRC [5]. In this study, this criterion was used. The same nominal MRC value for both systems was considered, 15.2 kg h^{-1}. The selected DX system was specifically designed to maintain indoor conditions in swimming pools and other high latent loads buildings, such as spas [33]. Both systems studied were not equipped with any humidifier element, since they were designed to handle very humid indoor air.

2.1.1 DX system

A numerical model of a DX system was created in order to compare its operational behaviour with the proposed DW-IEC system. The DX system was composed of an air-mixing box, a vapor-compression cycle and a heating coil, HC, see Fig. 1. The HC was fed by a constant water flow, which was heated using an air-water heat pump. The evaporator, EV, and the condenser, CO, of the vapor-compression cycle were installed in a parallel arrangement.

Air handling by the DX system is described below. Firstly, the outdoor air stream was mixed with the return air stream. Secondly, the mixed air stream was dehumidified and cooled by the evaporator, EV. Finally, the air stream was heated by the HC until the supply air temperature equalled the set point temperature. The supply air humidity ratio was controlled with the EV and the supply air temperature was controlled with the HC. The outdoor air flow rate of this system was 1600 m^3 h^{-1}, and the total air flow rate handled and supplied by the DX system was 3680 m^3 h^{-1}. The condenser, CO, of the direct expansion refrigeration unit handled 100% outdoor air, 3680 m^3 h^{-1}.

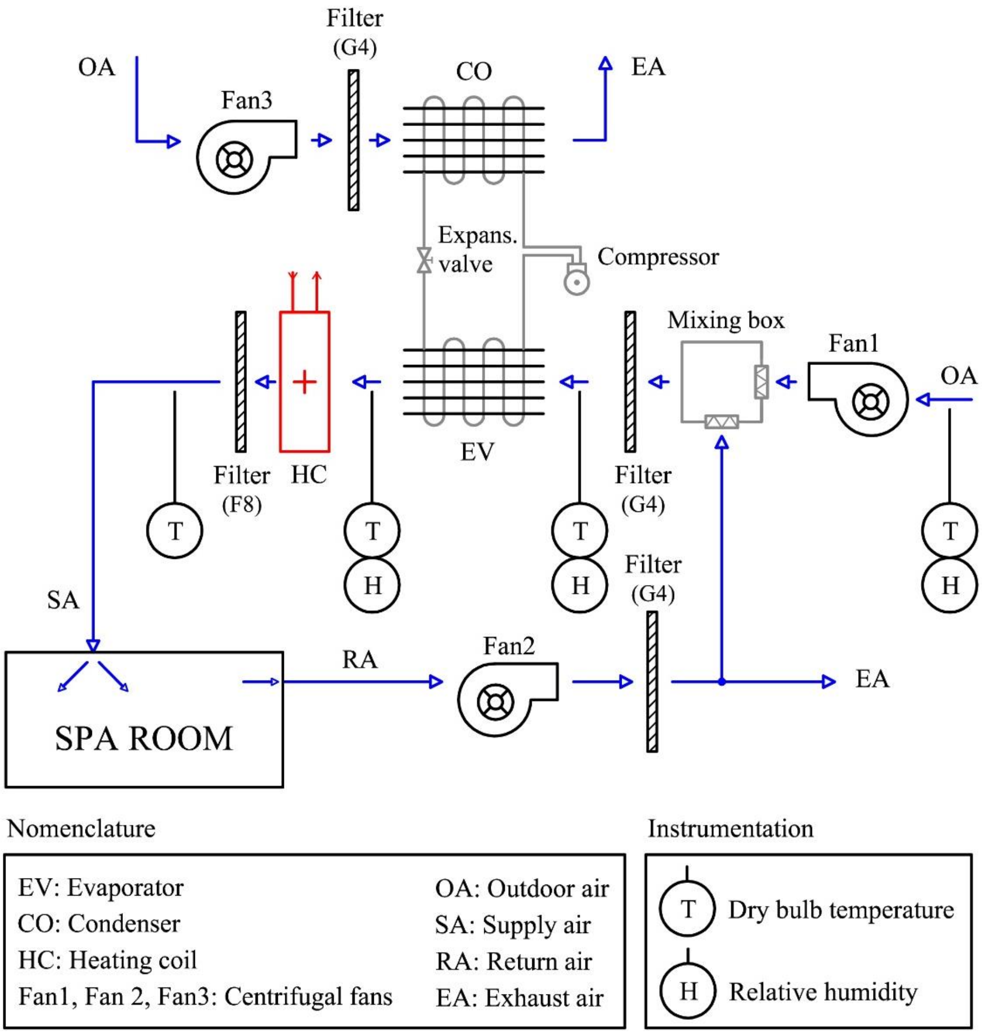

Fig. 1. Schematic of the DX system.

2.1.2 DW-IEC system

An alternative DW-IEC system was proposed in this piece of work in order to maintain the required indoor conditions in buildings with high latent loads. A schematic of the DW-IEC system is shown in Fig. 2. It is composed of a DW to handle latent heat loads in the room, and an IEC and a heating coil, HC2, to handle sensible heat loads. The DW was activated by means of a heating coil, HC1. Alternatively, the IEC was used as a sensible heat exchanger, SHE, recovering sensible heat from the return air stream, when it was necessary to heat the process air stream. In addition, two air boxes were integrated into the system to increase the desiccant and cooling capacity of the DW and the IEC, respectively. Both boxes have two air inlet dampers and one outlet. Depending on outdoor air conditions, the exhaust air stream is the outside, OA, air or return air, RA, as shown in Fig. 2. A constant air flow rate of 1600 $m^3\ h^{-1}$ was considered for the three air streams. The outdoor air flow rate of this system was equal to that of the DX system. Furthermore, this study was performed for relatively low regeneration air temperatures (40–60 ºC), which can be obtained using a commercial heat pump.

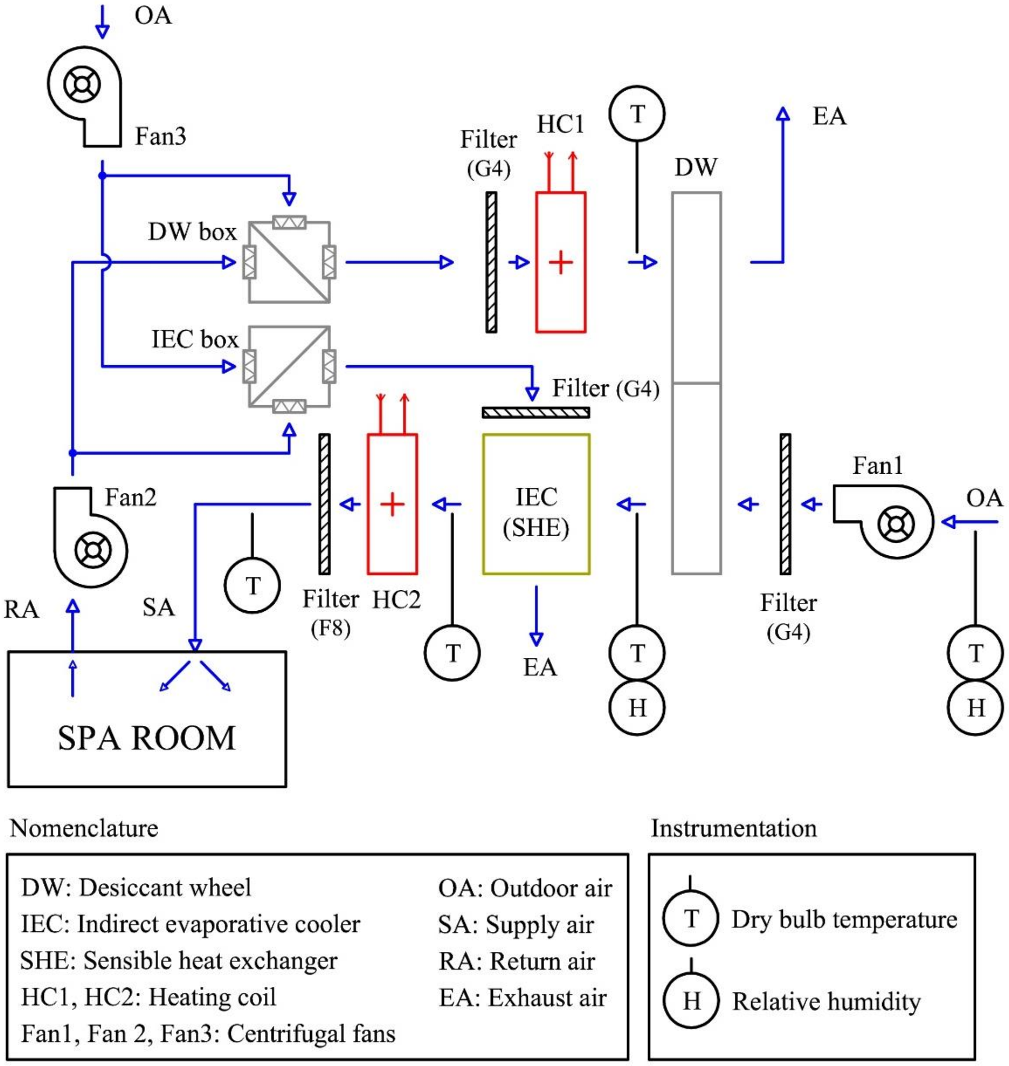

Fig. 2. Schematic of the DW-IEC system.

2.1.2.1 System operation modes

Two independent main control loops were considered in the DW-IEC system. The first one was an indoor air humidity control loop and the second one an indoor air temperature control loop. A diagram of the control logic of the DW-IEC system is represented in Fig. 3. The air humidity control loop was divided into two specific modes of operation, Mode 1-H and 2-H. This loop modulated the water flow rate of the regeneration heating coil, HC1, activated the rotation of the DW and set the position of the dampers in the DW and IEC boxes. The air temperature control loop was divided into three specific modes of operation, Mode 1-T, 2-T and 3-T. This loop modulated the water flow rate of the IEC and the post-heating coil, HC2. These modes of operation are described below.

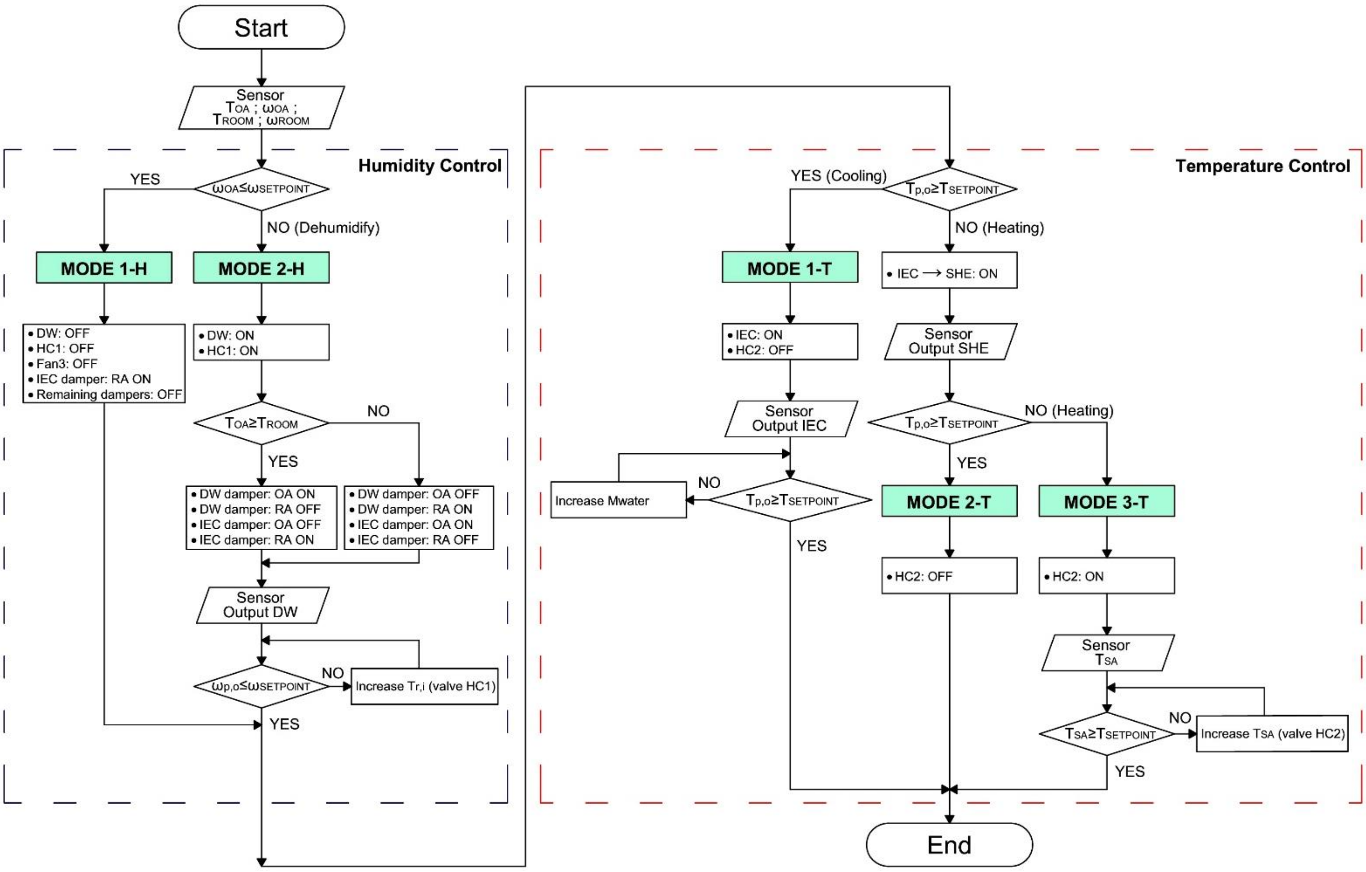

Fig. 3. DW-IEC system control logic diagram.

- **Air humidity control**

The operating mode of the selected humidity control was based on the outdoor air humidity ratio, ω_{OA}. The DW-IEC system did not dehumidify when the outdoor air humidity was lower than the set point air humidity. Mode 1-H was activated, see Fig. 2 and Fig. 3. For this operating mode, the DW, HC1 and Fan3 elements were disabled, and as a result the supply air humidity ratio was equal to the outdoor air humidity ratio. On the contrary, the DW-IEC system dehumidified when the outdoor air humidity was higher than the set point air humidity, and Mode 2-H was activated.

For this control mode, the system dehumidified the outdoor air until the outlet process air humidity ratio of the DW, $\omega_{p,o,}$ was equal to or lower than the set point humidity. The DW, HC1 and Fan3 elements were activated and the dampers of the two air boxes were set to the correct position, see Fig. 2 and Fig. 3. The outdoor air, OA, passed through DW damper and the return air, RA, passed through IEC damper when the outdoor air temperature was higher than the set point air temperature. On the contrary, the outdoor air, OA, passed through IEC damper and the return air, RA, passed through DW damper.

- **Air temperature control**

The operating mode of the selected temperature control was based on the DW outlet process air temperature, $T_{p,o}$. Mode 1-T was activated when $T_{p,o}$ was higher than the set point air temperature, see Fig. 2 and Fig. 3. The IEC system was activated until the set point temperature of the process air steam was achieved. The process air stream was heated when $T_{p,o}$ of the DW was lower than the set point air temperature. The outlet process air stream of the DW can be heated by the sensible heat exchanger, SHE. The IEC was only used as SHE when the rotation of the DW was disabled and the secondary air stream was return air. In this situation, no water was evaporated in the SHE. Then, the air temperature was measured again at the output of the IEC unit, see Fig. 2 and Fig. 3. The primary air stream of the IEC was supplied to the building when $T_{p,o}$ was higher than the set point air temperature, and the HC2 was off, Mode 2-T. However, HC2 was activated when $T_{p,o}$ was lower than the set point air temperature and the air stream was heated until the supply air temperature was equal to the set point temperature, Mode 3-T.

2.2 Building model – Spa

Both HVAC systems were designed to serve air in a building with high latent loads. A building model was designed to simulate the thermal behaviour of a spa. This was modelled and simulated using TRNSYS package tool [34]. The building consisted of a single surface of 64 m^2 and a height of 3.9 m, where a wall, south orientation, and the roof were exterior. The characteristics of the building are summarized in Table 1.

The building was composed of a swimming pool of 32 m^2 and a daily maximum number of 8 people in the pool. The evaporated water flow rate from the pool was calculated using Eq. (1), according to that established in [5]. Where S is the pool area, ω_w is the saturated air humidity ratio at the pool water temperature, ω_{IA} is the indoor air humidity ratio and Np is the number of people. Other internal energy gains due to people and lighting were considered, as shown in Table 1.

$$\dot{M}_{pool} = S \cdot \left(16 + 133 \cdot \frac{Np}{S}\right) \cdot (\omega_w - \omega_{IA}) + 0.1 \cdot Np \qquad (1)$$

Based on the Spanish regulations on thermal installations in buildings [35], the indoor air temperature set for swimming pools should be between 1 and 2 °C above the pool water temperature, with a maximum of 30 °C, and the indoor relative humidity should be maintained below 65 %. In this paper, the indoor conditions were set at 27 ºC for the air temperature and 60 % for the relative humidity. The building was simulated for a daily operating schedule from 09:00 am to 24:00 pm.

Table 1. Characteristics of the building.

Building	Floor area	64 m^2
	Height	3.9 m
	Exterior wall area	31.2 m^2
	Exterior roof area	64 m^2
	Indoor air temperature	27 ºC
	Indoor relative humidity	60 %
Pool	Area	32 m^2
	Water temperature	25 ºC
U-value	Exterior wall	0.339 W m^{-2} K^{-1}
	Roof	0.313 W m^{-2} K^{-1}
Heat gain	Pool	Latent: 6662 W ($\dot{M}_{pool}$=9.6 kg h^{-1})
	Lighting	55 W m^{-2} (50 % convective part)
	People	8 persons
		Sensible: 75 W/person
		Latent: 75 W/person
Daily schedule	09:00 am to 24:00 pm	

2.3 Components modelling

The components that compose the proposed DW-IEC system and the DX system, were modelled as described below. Each of the component models was combined and integrated into TRNSYS [34]. The models of the DW, the IEC, the refrigeration vapour compression unit, the heat pump and the fans were validated experimentally. These models were fitted by first, second and third order polynomial equations, expressed by Eqs. (2)-(4), respectively, where Ŷ is the estimated output value, X are input variables, b_i, b_{ii}, b_{iii} and b_{ij} are the estimated parameters of linear, quadratic, cubic and the second-order terms, respectively, and b_0 is the average response in the model.

$$\hat{Y} = b_0 + \sum_{i=1}^{k} b_i \cdot X_i \tag{2}$$

$$\hat{Y} = b_0 + \sum_{i=1}^{k} b_i \cdot X_i + \sum_{i=1}^{k} b_{ii} \cdot X_i^2 \tag{3}$$

$$\hat{Y} = b_0 + \sum_{i=1}^{k} b_i \cdot X_i + \sum_{i=1}^{k} b_{ii} \cdot X_i^2 + \sum_{i=1}^{k=1} b_{iii} \cdot X_i^3 \tag{4}$$

2.3.1 Desiccant wheel model

The desiccant wheel model behaviour was studied in a previous paper [17]. This model was based on the statistical technique of design of experiments. The model was adjusted to obtain the outlet process air temperature and humidity ratio in the DW, $T_{p,o}$ and $\omega_{p,o}$, especially for low regeneration temperature activated systems. The input variables of the model were the inlet process air temperature and humidity ratio, $T_{p,i}$ and $\omega_{p,i}$, the inlet regeneration air temperature and humidity ratio, $T_{r,i}$ and $\omega_{r,i}$, and the process specific mass air flow rate, $\Omega_{p,i}$. In this study, the process and regeneration specific mass air flow rates were always maintained constant, 21.51 kg s^{-1} m^{-3}. The relationship between the output and input variables was examined using second order polynomial equations, expressed by Eq. (3). The corresponding estimated parameters of the DW model are shown in Table 2.

Table 2. Estimated parameters of the DW empirical model.

b_x	X_i	$T_{p,o}$x10^3 [ºC]	$\omega_{p,o}$x10^3 [g kg^{-1}]	b_x	X_i	$T_{p,o}$x10^3 [ºC]	$\omega_{p,o}$x10^3 [g kg^{-1}]
b_0	-	-6736.67	-15366.80	b_{11}	$\omega_{p,i}^2$	-17.23	16.76
b_1	$T_{p,i}$	72.10	1277.57	b_{12}	$\omega_{p,i}\cdot T_{r,i}$	-1.49	-2.23
b_2	$\omega_{p,i}$	772.28	-785.18	b_{13}	$\omega_{p,i}\cdot\omega_{r,i}$	5.65	16.84
b_3	$T_{r,i}$	410.38	1310.33	b_{14}	$\omega_{p,i}\cdot\Omega_{p,i}$	20.50	-6.79
b_4	$\omega_{r,i}$	224.17	-916.88	b_{15}	$T_{r,i}^2$	-5.09	-11.90
b_5	$\Omega_{p,i}$	357.36	-94.71	b_{16}	$T_{r,i}\cdot\omega_{r,i}$	7.31	-10.40
b_6	$T_{p,i}^2$	16.58	-28.38	b_{17}	$T_{r,i}\cdot\Omega_{p,i}$	6.71	-3.50
b_7	$T_{p,i}\cdot\omega_{p,i}$	-14.35	29.84	b_{18}	$\omega_{r,i}^2$	-9.72	24.41
b_8	$T_{p,i}\cdot T_{r,i}$	7.35	-10.61	b_{19}	$\omega_{r,i}\cdot\Omega_{p,i}$	-5.49	11.88
b_9	$T_{p,i}\cdot\omega_{r,i}$	-12.93	6.35	b_{20}	$\Omega_{p,i}^2$	-12.17	-9.44
b_{10}	$T_{p,i}\cdot\Omega_{p,i}$	-8.71	5.89	-	-	-	-

2.3.1 Indirect evaporative cooler model

The model used to study the behaviour of the IEC was studied in a previous paper [36] and was based on the statistical technique of design of experiments, as well as the model used for the DW. The IEC empirical model was able to accurately predict the outlet primary air temperature, $T_{p,o}$, the outlet secondary air temperature, $T_{s,o}$, and the outlet secondary air humidity ratio of the system, $\omega_{s,o}$, under different operating conditions. The input variables were the inlet primary air temperature, $T_{p,i}$, the inlet secondary air temperature, $T_{s,i}$, the inlet secondary air humidity ratio, $\omega_{s,i}$, the secondary air velocity, v_s, and the water flow rate, $\dot{V}_w$. The relationship between the input and output variables was expressed by Eq. (2). The corresponding estimated parameters of the IEC model are shown in Table 3.

Table 3. Estimated parameters of the IEC empirical model.

b_x	X_i	$T_{p,o}$ x10^3 [ºC]	$T_{s,o}$ x10^3 [ºC]	$\omega_{s,o}$ x10^3 [g kg^{-1}]	b_x	X_i	$T_{p,o}$ x10^3 [ºC]	$T_{s,o}$ x10^3 [ºC]	$\omega_{s,o}$ x10^3 [g kg^{-1}]
b_0	-	-1313.76	3801.74	-379.62	b_8	$T_{p,i}\cdot v_s$	-15.66	-25.34	-35.06
b_1	$T_{p,i}$	322.41	500.49	183.23	b_9	$T_{p,i}\cdot\dot{V}_w$	-1.23	-2.02	1.12
b_2	$T_{s,i}$	364.07	191.57	135.71	b_{10}	$T_{s,i}\cdot\omega_{s,i}$	-8.45	-5.85	3.32
b_3	$\omega_{s,i}$	766.52	455.43	313.29	b_{11}	$T_{s,i}\cdot v_s$	26.11	42.55	-6.63
b_4	v_s	-467.09	-1199.63	755.41	b_{12}	$T_{s,i}\cdot\dot{V}_w$	-2.11	-1.54	0.92
b_5	$\dot{V}_w$	41.87	20.99	3.33	b_{13}	$\omega_{s,i}\cdot v_s$	12.58	19.45	33.91
b_6	$T_{p,i}\cdot T_{s,i}$	0.42	0.60	0.19	b_{14}	$\omega_{s,i}\cdot\dot{V}_w$	2.87	3.37	-2.39
b_7	$T_{p,i}\cdot\omega_{s,i}$	-5.09	-3.93	6.28	b_{15}	$v_s\cdot\dot{V}_w$	-0.94	3.94	-4.54

The IEC was used as a SHE when it was necessary to heat the process air stream and not to cool it, as was mentioned previously. For this reason, a cross flow sensible heat exchanger with both hot and cold sides unmixed, was modelled. The physical design characteristics of SHE were similar to those of the IEC [36]. The effectiveness of the SHE at each time step was calculated by

Eq. (5), where UA is the overall heat transfer coefficient of the exchanger, C_p is the capacity rate of air on primary side ($C_p = \dot{m}_p \cdot c_{p,p}$) and C_s is the capacity rate of air on secondary side ($C_s = \dot{m}_s \cdot c_{p,s}$). In this work, the effectiveness of the SHE was calculated for a fixed value of UA, given the inlet temperatures and air flow rates. The UA value of the cross-flow heat exchanger was measured experimentally for a wide range of input conditions, obtaining an average value of 1440 kJ h^{-1} K^{-1}.

$$\varepsilon = \frac{1 - \exp(-\frac{UA}{C_s} \cdot \left(1 + \frac{C_s}{C_p}\right))}{1 + \frac{C_s}{C_p}} \quad (5)$$

2.3.2 Refrigeration vapour compression model

The considered refrigeration vapour compression unit of the DX system was specially designed to dehumidify indoor swimming pools and other dehumidification applications. This unit was modelled using experimental data available from the manufacturer [33]. The unit works for balanced air flow rates in both coils, with a value of 3680 m^3 h^{-1}.

A simplified experimental model based on correlations was obtained to study its behaviour [37]. The relationship between the output and input variables was expressed by second order polynomial equations, as shown in Eq. (3). The input variables of this model were the inlet evaporator dry bulb air temperature, $T_{e,i}$, the inlet evaporator wet bulb air temperature, $T_{wb,e,i}$, the inlet condenser dry bulb air temperature, $T_{c,i}$, and the volumetric air flow rate ratio, $\dot{V}' = \dot{V}/\dot{V}_N$. The output variables were calculated using the following ratios: evaporator total heat transfer ratio $\dot{Q}'_{e,t} = \dot{Q}_{e,t}/\dot{Q}_{e,t,N}$; evaporator sensible heat transfer ratio $\dot{Q}'_{e,sen} = \dot{Q}_{e,sen}/\dot{Q}_{e,sen,N}$; condenser total heat transfer ratio $\dot{Q}'_{c,t} = \dot{Q}_{c,t}/\dot{Q}_{c,t,N}$; electric power consumption ratio $\dot{W}' = \dot{W}/\dot{W}_N$. Where $\dot{Q}_{e,t}$ is the evaporator total heat transfer, $\dot{Q}_{e,sen}$ is the evaporator sensible heat transfer, $\dot{Q}_{c,t}$ is the condenser total heat transfer and $\dot{W}$ is the electric power consumption of the compressor. The estimated parameters of the output variables are shown in Table 4. The nominal characteristics of the vapour compression system obtained experimentally by the manufacturer were used, see Table 5.

Table 4. Estimated parameters of the refrigeration vapour compression model.

b_x	X_i	$\dot{Q}'_{e,t}$ x10^3	$\dot{Q}'_{e,sen}$ x10^3	$\dot{Q}'_{c,t}$ x10^3	$\dot{W}'$ x10^3	b_x	X_i	$\dot{Q}'_{e,t}$ x10^3	$\dot{Q}'_{e,sen}$ x10^3	$\dot{Q}'_{c,t}$ x10^3	$\dot{W}'$ x10^3
b_0	-	145.20	202.46	264.37	622.12	b_8	$\dot{V}'^2$	-185.21	-249.68	-89.82	221.34
b_1	$T_{e,i}$	-1.79	33.88	-1.70	-1.00	b_9	$T_{e,i}\cdot T_{c,i}$	0.08	-0.28	0.09	0.09
b_2	$T_{c,i}$	8.45	8.93	7.82	7.34	b_{10}	$T_{e,i}\cdot T_{wb,e,i}$	-0.65	2.32	-0.56	-0.29
b_3	$T_{wb,e,i}$	17.71	-35.46	16.36	11.82	b_{11}	$T_{e,i}\cdot \dot{V}'$	3.55	57.59	2.77	0.18
b_4	$\dot{V}'$	475.27	610.50	280.22	-345.74	b_{12}	$T_{c,i}\cdot T_{wb,e,i}$	-0.34	0.46	-0.23	0.14
b_5	$T_{e,i}^2$	0.20	-0.95	0.18	0.09	b_{13}	$T_{c,i}\cdot \dot{V}'$	-0.29	-2.39	-1.24	-4.92
b_6	$T_{c,i}^2$	-0.24	-0.29	-0.12	0.27	b_{14}	$T_{wb,e,i}\cdot \dot{V}'$	3.97	-49.65	0.17	-11.94
b_7	$T_{wb,e,i}^2$	0.75	-1.81	0.66	0.39	-	-	-	-	-	-

Table 5. Nominal parameters of the refrigeration vapour compression system.

Parameters	Value	
$\dot{Q}_{e,t,N}$	23.06	[kW]
$\dot{Q}_{e,sen,N}$	13.00	[kW]
$\dot{Q}_{c,t,N}$	30.32	[kW]
$\dot{W}_N$	7.53	[kW]
$\dot{V}_N$	4600	[m^3 h^{-1}]

2.3.3 Heating coil with heat pump model

The heating coils of both systems studied, Fig. 1 and Fig. 2, were fed by a constant water flow, which was heated by an air-water heat pump. The thermal power exchanged by the heating coil was obtained by Eq. (6).

$$\dot{Q}_{HC} = \dot{V}_{a,i} \cdot \rho_{a,i} \cdot \left(h_{a,o} - h_{a,i}\right) \tag{6}$$

The selected air-water heat pump covered all the required sensible heat. This heat pump is fitted with a scroll inverter compressor. The technical characteristics of the heat pump were: a nominal heating capacity of 28.1 kW, a nominal electric power consumption 9.6 kW and a nominal COP of 2.93 [33]. In order to obtain the electric power consumption of the heat pump, the simplified experimental model obtained by the manufacturer was used [33]. The output variable of the model was the heating electrical input ratio, EIR, which is the inverse of COP. The estimate EIR value was calculated from Eq. (7), where EIR_N is its nominal value, EIR_T is a second order polynomial equation based on the outdoor air temperature and outlet water temperature, as shown in Eq. (3), and EIR_{PLF} is a third order polynomial based on the partial load factor, expressed by Eq. (4). The estimated parameters of the estimate EIR value are shown in Table 6.

$$EIR = EIR_N \cdot EIR_T \cdot EIR_{PLF} \tag{7}$$

Table 6. Estimated parameters of the air-water heat pump model.

b_x	X_i	EIR_T x10^3	b_x	X_i	EIR_{PLF} x10^3
b_0	-	805.57	b_0	-	30.39
b_1	$T_{w,o}$	-4.20	b_1	PLF	1518.51
b_2	$T_{w,o}^2$	0.11	b_2	PLF^2	-1323.27
b_3	T_{OA}	-5.68	b_3	PLF^3	774.38
b_4	T_{OA}^2	0.11	-	-	-
b_5	$T_{w,o} \cdot T_{OA}$	-0.15	-	-	-

2.3.4 Filter

Filters were characterized by a constant pressure drop in the air circuit. Several filters with F8 or G4 protection were considered, as shown in Fig. 1 and Fig. 2. The pressure drop of these filters are shown in Table 7. However, the increase of their pressure drop due to dust accumulation was not considered.

2.3.5 Fan model

The fans were sized to maintain the design air flow rate given the estimated system pressure drop. The air pressure drop of each component is shown in Table 7. The fans were modelled using manufacturer data from Sodeca QuickFan software [38]. Three centrifugal fans were selected for the DX system and another three for the DW-IEC system, as shown in Fig. 1 and Fig. 2. The return and exhaust fans of the DX systems were the same. These fans were also the same for the DW-IEC systems, but different from those of the DX system. The estimated parameters of the fan models are shown in Table 8, where the output variables were static pressure, P, and electric power consumption of the fans, $\dot{W}$. The relationship between the output and input variables was expressed by second order polynomials, according to Eq. (3).

Table 7. Pressure drop of each component for the systems analysed.

Component	Pressure drop [Pa]
Desiccant wheel (process side)	350
Desiccant wheel (regeneration side)	380
Indirect evaporative cooler	146
Evaporator	40
Condenser	27
Heating coil	35
Air box with dampers	40
Filter (G4 protection)	60
Filter (F8 protection)	100
Air duct	40

Table 8. Estimated parameters of the fan models.

		DX system				DW-IEC system			
		Fan1		Fan2 and Fan3		Fan1		Fan2 and Fan3	
b_x	X_i	P x10^3 [mmca]	$\dot{W}$ x10^3 [kW]	P x10^3 [mmca]	$\dot{W}$ x10^3 [kW]	P x10^3 [mmca]	$\dot{W}$ x10^3 [kW]	P x10^3 [mmca]	$\dot{W}$ x10^3 [kW]
b_0	-	35478.6	339.9	8824.7	162.2	191371	463.03	76510.9	194.7
b_1	$\dot{V}$	11.653	0.057	14.669	0.039	77.617	0.522	- 4.768	0.192
b_2	$\dot{V}^2$	0.004	-	- 0.004	-	-0.077	-	- 0.005	-

2.4 Climate zones

The performance of the DX and DW-IEC systems under several climatic conditions was evaluated according to ASHRAE climate classification [39]. This classification consists of 8 climate zones, depending on the cooling degrees-day and heating degrees-day. In this study, both systems were simulated for the climate zones 1 to 6, from very hot to cold. Climate zones 7 and 8, very cold and subarctic, respectively, were not used in this study because they are very dry, and therefore, do not require a dehumidification system. The simulations were performed using the Meteonorm weather data library [40]. One city from each of the 6 selected climate zones was chosen, see Table 9. A world map with the 6 selected cities is shown in Fig. 4, where the colour scale represents the different climate zones and subzones around the world.

Table 9. Selected cities from each of the climate zone defined by ASHRAE.

Climate zone[a]	City	Thermal criteria[b] [ºC]
1	Singapore	5000 < cooling degree-day
2	Taipei	3500 < cooling degree-day ≤ 5000
3	Tunis	cooling degree-day ≤ 2500 and heating degrees-day ≤ 2000
4	Barcelona	cooling degree-day ≤ 2500 and heating degrees-day ≤ 3000
5	Budapest	3000 < heating degrees-day ≤ 4000
6	Ottawa	4000 < heating degrees-day ≤ 5000

[a] 1- Very hot, 2- hot, 3- warm, 4- mixed, 5- cool, 6- cold

[b] T_{base}= 10ºC for cooling degree-day; T_{base}= 18ºC for heating degrees-day

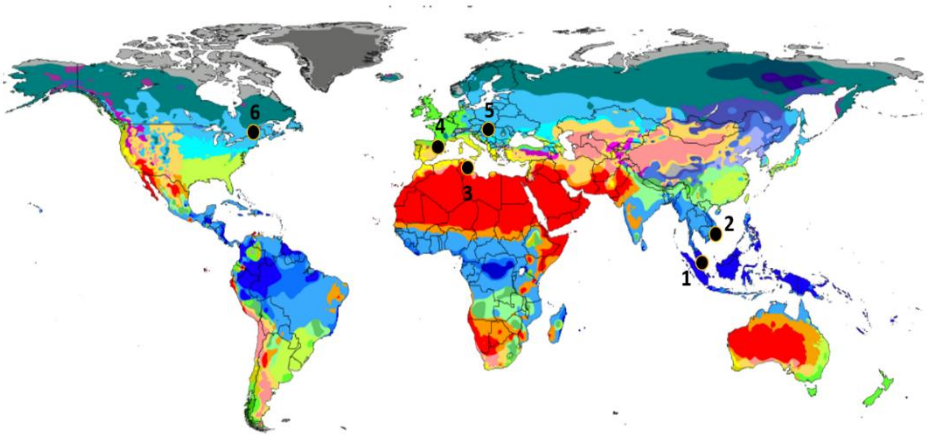

Fig. 4. World representation of the different climate zones with the selected cities.

2.5 Energy simulation

Several detailed energy simulations were carried out with the assumption that both HVAC systems served a spa with high latent loads. All the energy simulations were carried out with the TRNSYS 17 software [34], using a time step of 15 minutes. The simulations were performed for the selected six climate zones throughout the whole year.

The HVAC systems were evaluated according to the following parameters: electric power consumption, $\dot{W}$, sensible and latent energy delivered, $\dot{Q}_{sen}$ and $\dot{Q}_{lat}$, respectively, the seasonal mean coefficient of performance, SCOP, expressed by Eq. (8), and the energy consumption per unit of dehumidified water, E_{cons}, expressed by Eq. (9). The latter was calculated from the $\dot{W}$ and MRC parameters of the HVAC system, only when it was in dehumidification mode, i.e. when air dehumidification was demanded by the system.

$$SCOP = \frac{\int\left(\dot{Q}_{sen} + \dot{Q}_{lat}\right) dt}{\int \dot{W}\, dt} \tag{8}$$

$$E_{cons} = \frac{\int \dot{W}\, dt}{\int MRC\, dt} \tag{9}$$

3 Results and analysis

The energy analysis of the simulations is presented in daily, monthly and annual analysis to correctly understand the behaviour of both HVAC systems.

3.1 Daily behaviour analysis

The daily analysis was performed for the climatic conditions of Barcelona. A typical winter day, January 10th, and a typical summer day, July 10th, were selected.

3.1.1 Daily behaviour of the DX system

The thermal behaviour and energy consumption of the DX system for a typical winter day and a typical summer day are represented in Fig. 5. Regarding the winter day, in the first process of the DX system, the outdoor air stream was mixed with return air stream, increasing its temperature and humidity, see Fig. 5a. Nevertheless, this humidity was lower than the set point air humidity, therefore the dehumidification mode was not activated and the air stream was not handled by the

EV. The mixing air stream was heated by the HC until the set point temperature value was achieved, and finally supplied to the building. The energy consumption values of the compressor and Fan 3 were equal to zero, as air dehumidification was not required, see Fig. 5b. The energy consumption of the HC was reduced when the outdoor temperature increased and the partial load factor of the heat pump decreased. Regarding the summer day, the mixing process also raised the humidity, therefore it was necessary to activate the dehumidification mode it order to reduce it, see Fig. 5c. The mixing air stream was dehumidified and cooled by the EV until the set point humidity was achieved. Then, the dry air flow was heated by the HC and supplied to the building. In this case study, the compressor consumed a significant amount of energy, as the latent energy required by the EV was high, Fig. 5d. The fans maintained low and constant energy consumption values throughout the day, and small oscillations were found for the HC.

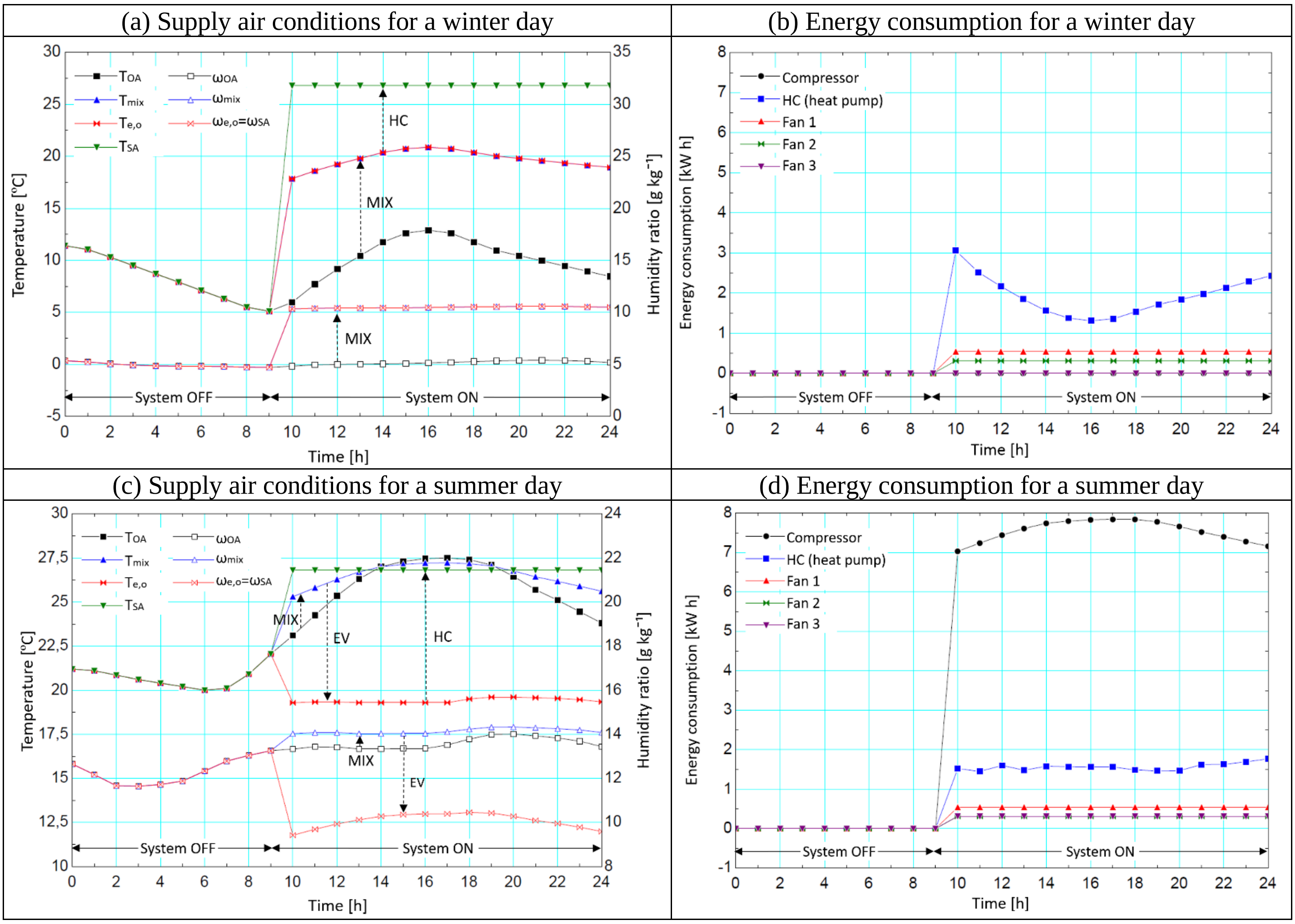

Fig. 5. Daily operational characteristics of the DX system for the climatic conditions of Barcelona.

3.1.2 Daily behaviour of the DW-IEC system

The results of the daily simulations for the DW-IEC system on a typical winter day and a typical summer day in Barcelona are represented in Fig. 6. Regarding the winter day, the outdoor air humidity was lower than the set point air humidity, see Fig. 6a, so air dehumidification was not necessary and the mode of operation Mode 1-H was activated, deactivating the DW, HC1 and Fan3, see Fig. 3. In this case, the outdoor humidity was the supply humidity. Then, the air process stream was handled by the IEC unit, which was used as a SHE, recovering sensible heat from the return air stream. However, the outlet air temperature of the SHE was lower than the set point temperature, so a post-heating by HC2 was required to increase the air temperature, according to Mode 3-T. As a result of this, the energy consumption of the DW, HC1 and Fan3 were zero, the energy consumption of HC2 varied according to the outdoor air temperature and the PLF values of the heat pump, and the energy consumption of Fan 1 and Fan 3 were constant throughout the day, see Fig. 6b. The highest energy consumption values were those of Fan 1, due to the process side pressure losses.

On the summer day analysed, the outdoor air humidity was higher than the set point humidity, see Fig. 6c, so the Mode 2-H control activates the DW and HC1. All simulations were carried out under assumption that the DW is regenerated with air heated to relatively low temperature values (40–60 ºC). The outlet process air temperature of the DW was higher than the set point air temperature. Therefore, Mode 1-T was activated and the process air stream was cooled by the IEC, thus achieving the set point air conditions and supplying the air stream to the building. HC1 showed the highest energy consumption values for the summer day, due to the regeneration energy required by the DW. The energy consumption of post-heating by HC2 was not required, so this was zero.

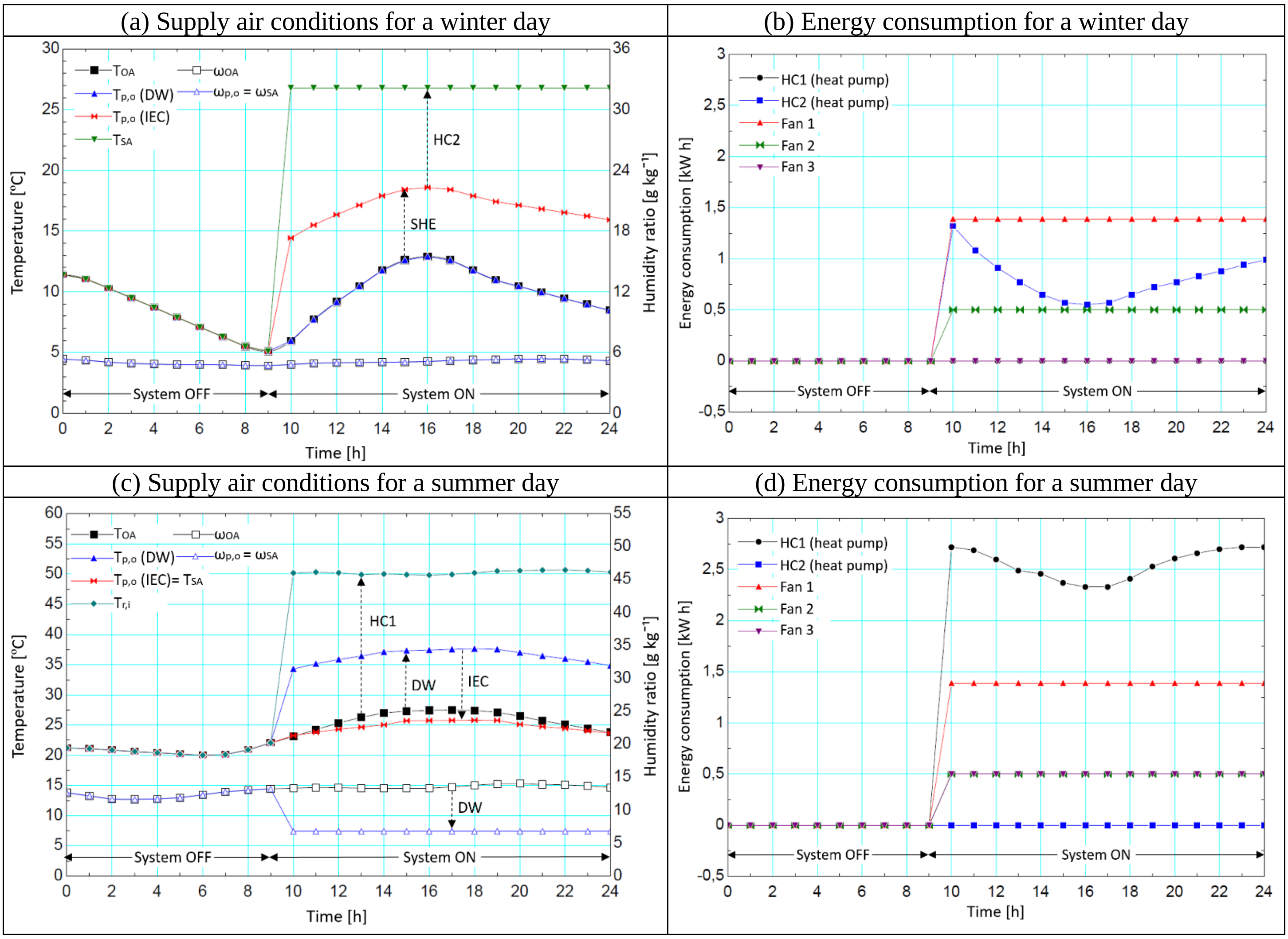

Fig. 6. Daily operational characteristics of the DW-IEC system for the climatic conditions of Barcelona.

It can be observed that the supply air humidity of the DW-IEC system was lower than the supply air humidity of the DX system, because the process air flow rate of the DW-IEC system was lower than that of the DX system. Thus, the latent energy delivered to the building with both systems was similar.

These case studies show that the modes of operation set for both systems provided the required indoor air conditions in the building in every season.

3.2 Monthly energy analysis

A monthly energy analysis for both HVAC systems for the climatic conditions of Barcelona was performed. Monthly sensible and latent energy delivered and monthly energy consumption by the DX and DW-IEC systems were obtained.

3.2.1 Monthly energy analysis of the DX system

The sensible and latent energy delivered of the DX system for the climatic conditions of Barcelona, climate zone 4, are represented in Fig. 7. This figure shows energy delivered of each element and the total monthly energy. The negative energy values indicate that the elements reduced the air temperature and humidity ratio, and the positive energy values indicate that the elements increased the air temperature and humidity ratio. It can be observed that the process of mixing air slightly increased the sensible energy delivered, see Fig. 7a, thus increasing the outlet air temperature of the mixing box. This process caused the sensible energy required by the HC to decrease, especially in January and December, where the sensible energy delivered in the process of mixing air is greater than in the remaining months, 7.2 kWh m^{-2} and 7.5 kWh m^{-2}, respectively. However, the mixing air also increased the latent energy delivered, see Fig. 7b, thus increasing the outlet air humidity of the mixing box. For example, the latent energy values delivered in January and December were 15.2 kWh m^{-2} and 16.2 kWh m^{-2}, respectively. Therefore, the mixing air did not improve the dehumidification system performance for the climate conditions of Barcelona.

The EV delivered sensible and latent energy during the months with dehumidification demand, i.e. when the mixed air humidity ratio was higher than the set point air humidity ratio, from April to November. The maximum sensible and latent energy values delivered by the EV were obtained in July and August. The building did not require dehumidification from December to March, therefore, the sensible and latent energy delivered by the EV was zero.

The sensible energy delivered by the HC was maintained throughout the year, due to the heating demand, i.e. when the inlet air temperature to the HC was lower than the set point air temperature.

This temperature was lower the set point air temperature from November to April, due mainly to the outdoor air, and from May to October, due to the low outlet air temperature of the EV.

Finally, it can be observed that the annual sensible and latent energy values delivered by the DX system were 365.7 kWh m^{-2} year^{-1} and -260.2 kWh m^{-2} year^{-1}, respectively.

(a)

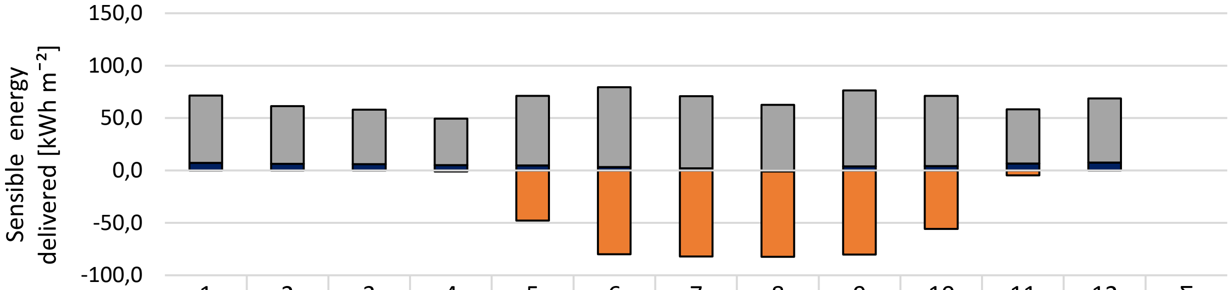

	1	2	3	4	5	6	7	8	9	10	11	12	∑
HC	64,3	55,2	52,1	44,2	66,3	76,2	68,8	62,5	72,7	66,9	51,8	61,1	742,1
EV	0,0	0,0	0,0	-0,9	-47,8	-79,9	-82,1	-81,2	-80,2	-55,6	-4,6	0,0	-432,3
MIX	7,2	6,2	6,0	5,2	4,9	3,3	2,0	-1,1	3,8	4,2	6,6	7,5	55,9
∑	71,5	61,4	58,1	48,6	23,4	-0,4	-11,3	-19,8	-3,7	15,5	53,8	68,6	365,7

(b)

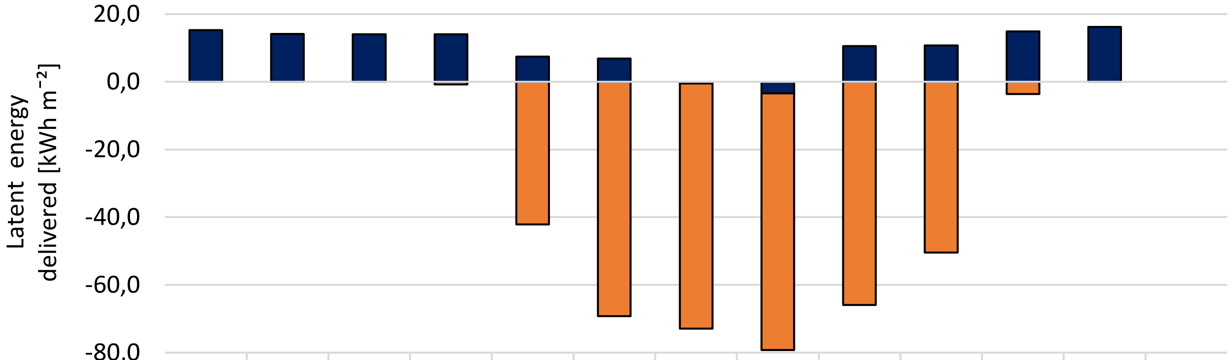

	1	2	3	4	5	6	7	8	9	10	11	12	∑
EV	0,0	0,0	0,0	-0,8	-42,2	-69,2	-72,4	-75,8	-65,9	-50,4	-3,6	0,0	-380,4
MIX	15,2	14,1	14,0	14,0	7,5	6,8	-0,5	-3,4	10,5	10,7	14,8	16,2	120,2
∑	15,2	14,1	14,0	13,3	-34,7	-62,4	-72,9	-79,2	-55,4	-39,7	11,2	16,2	-260,2

Fig. 7. Energy delivered by each element for the DX system for the climatic conditions of Barcelona, (a) sensible energy delivered and (b) latent energy delivered.

The monthly energy consumption of the DX system is represented in Fig. 8. This figure shows the monthly energy consumption of each element and the total monthly consumption. It can be observed that the highest energy consumption values were those for the compressor, which was activated during the months with dehumidification demand. The operation Fan3 was linked to that of the compressor, see Fig. 1, therefore, the energy consumption of Fan3 was zero during the months that the compressor was not in operation, from December to March. The energy consumption of the HC was maintained throughout the year, due to its sensible energy demand, as shown in Fig. 7a. The energy consumption of the HC was that of the heat pump. Regarding the monthly energy consumption, the maximum values were found from May to October, due mainly to the high dehumidification demand. The energy consumption was less during cold months with high heating demand, from November to February, and warm months, such as March and April. It can also be observed that the annual energy consumption for the climatic conditions of Barcelona with the DX system was 493.1 kWh m^{-2} $year^{-1}$, see Fig. 8.

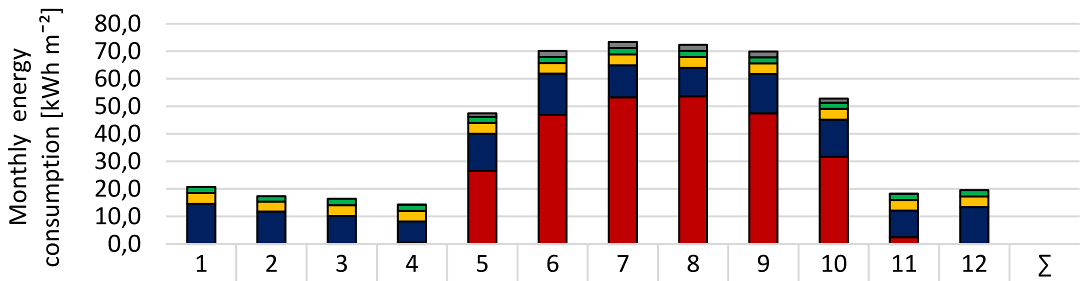

	1	2	3	4	5	6	7	8	9	10	11	12	∑
Fan3	0,0	0,0	0,0	0,0	1,3	2,2	2,3	2,3	2,1	1,5	0,1	0,0	11,8
Fan2	2,3	2,0	2,3	2,2	2,3	2,2	2,3	2,3	2,2	2,3	2,2	2,3	26,6
Fan1	3,9	3,6	3,9	3,8	3,9	3,8	3,9	3,9	3,8	3,9	3,8	3,9	46,3
HC	14,6	11,8	10,2	7,8	13,5	15,0	11,6	10,3	14,3	13,5	9,7	13,4	145,8
Compr	0,0	0,0	0,0	0,5	26,6	46,9	53,3	53,6	47,5	31,7	2,5	0,0	262,6
∑	20,8	17,4	16,4	14,2	47,6	70,1	73,4	72,4	70,0	52,9	18,3	19,6	493,1

Month

Fig. 8. Monthly energy consumption of each element for the DX system for the climatic conditions of Barcelona.

3.2.2 Monthly energy analysis of the DW-IEC system

The sensible and latent energy delivered of the DW-IEC system for the climatic conditions of Barcelona is shown in Fig. 9, broken down by the elements. It can be observed that the DW delivered high latent energy values from April to November, as shown in Fig. 9b, due to the dehumidification demand. The peak values, corresponding to July and August, are due to the high outdoor air humidity. The operation of HC1 was linked to that of the DW, in order to regenerate it, see Fig. 2 and Fig. 3. The sensible energy of HC1 was not delivered to the building, but outside.

The activation of the IEC was caused by the sensible energy delivered during the dehumidification process of the DW. As a consequence, sensible energy delivered by the IEC is obtained from April to November, in order to reduce the process air temperature, see Fig. 9a. The SHE recovered a large amount of energy during the months with heating demand and the DW was not in operation, thus reducing the energy required by HC2. The highest sensible energy values delivered by HC2 was found during the months with high heating demand, from November to March, months with low outdoor temperatures. Nevertheless, the sensible energy delivered by HC2 was zero from June to September, as shown in Fig. 9a.

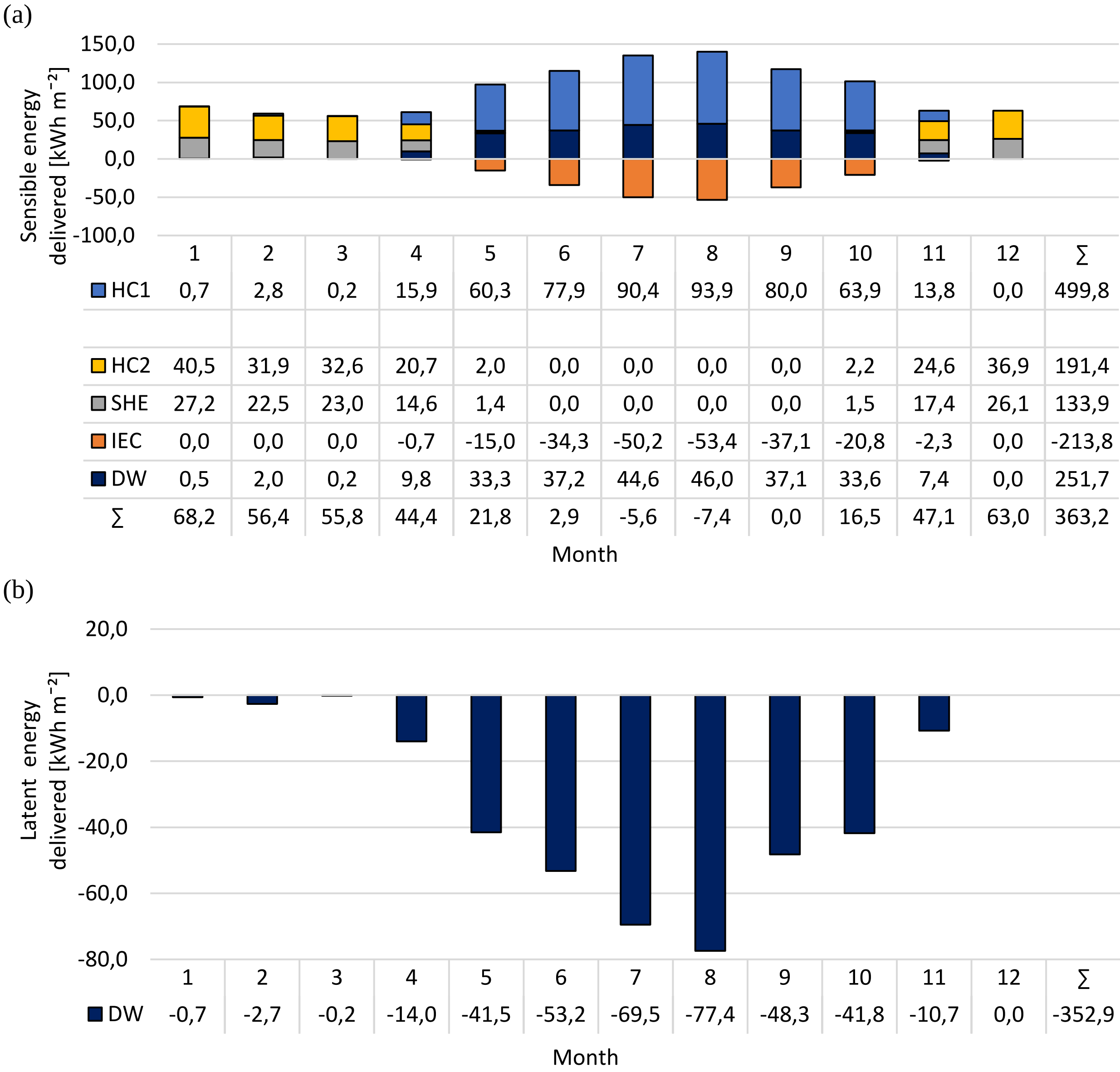

(a)

	1	2	3	4	5	6	7	8	9	10	11	12	∑
HC1	0,7	2,8	0,2	15,9	60,3	77,9	90,4	93,9	80,0	63,9	13,8	0,0	499,8
HC2	40,5	31,9	32,6	20,7	2,0	0,0	0,0	0,0	0,0	2,2	24,6	36,9	191,4
SHE	27,2	22,5	23,0	14,6	1,4	0,0	0,0	0,0	0,0	1,5	17,4	26,1	133,9
IEC	0,0	0,0	0,0	-0,7	-15,0	-34,3	-50,2	-53,4	-37,1	-20,8	-2,3	0,0	-213,8
DW	0,5	2,0	0,2	9,8	33,3	37,2	44,6	46,0	37,1	33,6	7,4	0,0	251,7
∑	68,2	56,4	55,8	44,4	21,8	2,9	-5,6	-7,4	0,0	16,5	47,1	63,0	363,2

(b)

	1	2	3	4	5	6	7	8	9	10	11	12	∑
DW	-0,7	-2,7	-0,2	-14,0	-41,5	-53,2	-69,5	-77,4	-48,3	-41,8	-10,7	0,0	-352,9

Fig. 9. Energy delivered by each element for the DW-IEC system for the climatic conditions of Barcelona, (a) sensible energy delivered and (b) latent energy delivered.

Finally, comparing these results with those obtained with the DX system, it can be observed that the monthly sensible and latent energy delivered to the building by each system was similar, see Fig. 7 and Fig. 9. The slight variations in the energy values delivered between both systems were mainly due to the different control systems used.

The monthly energy consumption by each element of the DW-IEC system are shown in Fig. 10. It can be observed that the element with the highest energy consumption values throughout the year was Fan1, 119.1 kWh m^{-2}, due to the high pressure drop of the proposed system. High energy consumption values by HC1 were found during the months with high dehumidification demand, from April to November. However, very low dehumidification demand was obtained from December to March, so the monthly energy consumption values by HC1 were very low or zero, see Fig. 10. The energy consumption of HC1 and HC2 were those of the heat pump. It can also be observed that the trend of energy consumption by HC2 was contrary to that of HC1. The highest energy consumption values by HC2 were found November to April, due to the heating demand, and the lowest values from May to October, because the outlet process air temperature of the DW was usually higher than the set point air temperature. The energy consumption of Fan3 was very low during the months that the DW was not in operation, since the operation of Fan2 was linked to that of the DW, see Fig. 2 and Fig. 3. The maximum monthly energy consumption values were found from May to October, due mainly to the high dehumidification demand, and then, as with the DX system. Finally, the annual energy consumption for the climatic conditions of Barcelona with the proposed DW-IEC system was 314.7 kWh m^{-2} $year^{-1}$, as shown in Fig. 10. Therefore, the annual energy consumption of the DW-IEC system was 36.2 % lower than that of the DX system for the climatic conditions of Barcelona, see Fig. 8 and Fig. 10.

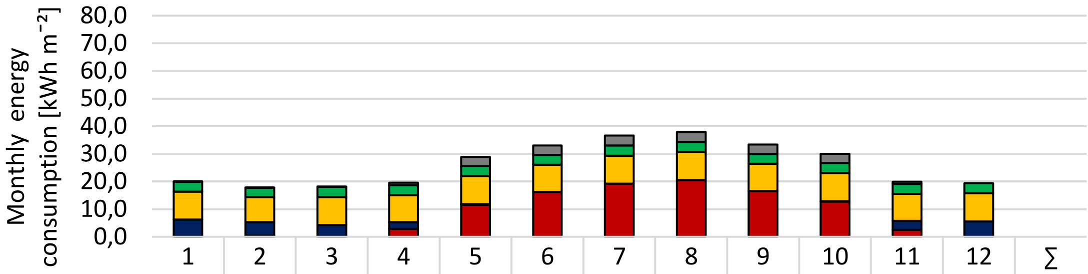

	1	2	3	4	5	6	7	8	9	10	11	12	∑
Fan3	0,0	0,2	0,0	1,0	3,4	3,5	3,6	3,6	3,5	3,3	0,8	0,0	23,1
Fan2	3,6	3,3	3,6	3,5	3,6	3,5	3,6	3,6	3,5	3,6	3,5	3,6	42,9
Fan1	10,1	9,1	10,1	9,8	10,1	9,8	10,1	10,1	9,8	10,1	9,8	10,1	119,1
HC2	6,1	4,8	4,2	2,5	0,2	0,0	0,0	0,0	0,0	0,2	3,2	5,6	26,8
HC1	0,1	0,5	0,0	2,8	11,5	16,2	19,2	20,5	16,6	12,7	2,5	0,0	102,8
∑	20,0	17,9	18,1	19,6	28,9	33,1	36,7	37,9	33,4	30,0	19,9	19,4	314,7

Month

Fig. 10. Monthly energy consumption for the DW-IEC system for the climatic conditions of Barcelona.

3.3 Annual energy analysis

In this section, the annual energy consumption of the proposed DW-IEC system was compared with those of the DX system. The comparative analysis was carried out for the 6 climate zones, as shown in Table 9.

3.3.1 Annual energy consumption

The operating annual energy consumption of both systems for the 6 climate zones is shown in Fig. 11. It can be observed that the maximum annual consumption values for both systems were obtained for the climate zone 1, a very hot climate zone, due to the high dehumidification demand. The energy consumption values were significantly reduced for cool climatic conditions, such as in climate zone 5. The consumption decreased by 51 % and 37 % between the climate zone 1 and 5 for the DX system and the DW-IEC system, respectively. However, the annual energy consumption values increased for climate zone 6, a cold climate zone, compared to those of zones 3, 4 and 5. This increase was caused mainly by the high heating demand. This trend of annual energy consumption was also obtained for the monthly energy consumption analysed in section 3.2, where the highest monthly consumption values were found for the months with high dehumidification demand, then, the months with high heating demand and finally, the remaining months.

It can be observed that the annual energy consumption of the DW-IEC system was always lower than that of the DX system, obtaining significant energy savings, always over 27.8 %, see Fig. 11. The highest energy savings were found for the climate zones with the highest annual energy consumption and the highest dehumidification demand, zones 1 and 2, with 43.5 % and 46.8 %, respectively.

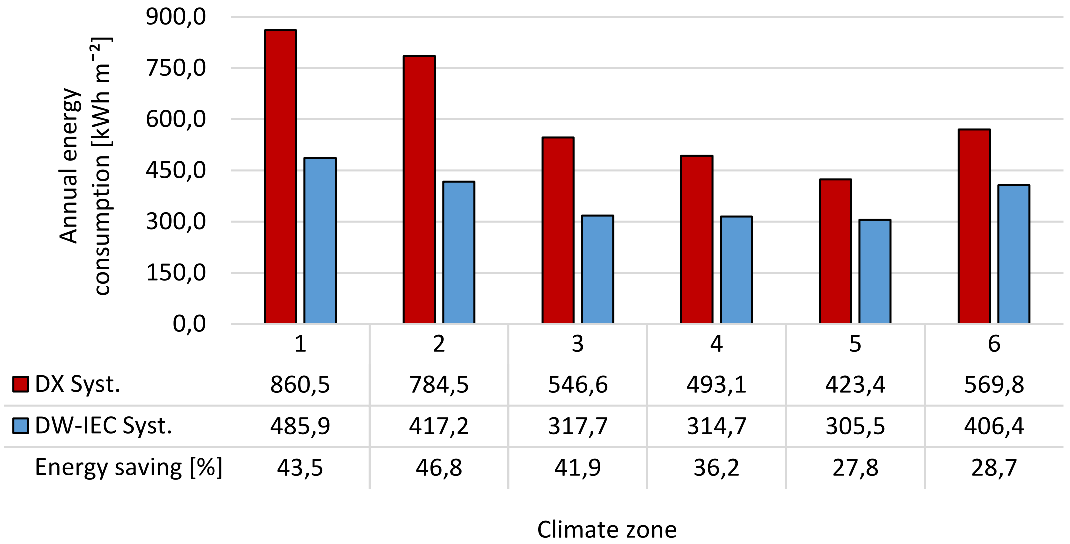

Fig. 11. Comparative analysis of annual energy consumption of the DW-IEC system and the DX system in each climate zone.

3.3.2 Seasonal mean coefficient of performance

The seasonal mean coefficient of performance, SCOP, of both systems, was calculated using Eq. (8). The SCOP values for the 6 climate zones are represented in Fig. 12. It can be observed that the maximum SCOP value for the DX system was 1.9, obtained from a cool climate zone, zone 5. Nevertheless, the maximum SCOP value for the DW-IEC system was 2.8, obtained from a very hot climate zone, zone 1.

The SCOP values of the DW-IEC system were always higher than that of the DX system, always over 27 %, as shown in Fig. 12. The greatest differences in SCOP between both systems, ΔSCOP, were found for climate zones 1 and 2, and the lowest for climate zones 5 and 6. The trend of

ΔSCOP was similar to the trend of annual energy saving, as shown in Fig. 11, since the sensible and latent energy delivered to the building by each system were the same, so ΔSCOP depended exclusively on energy consumption.

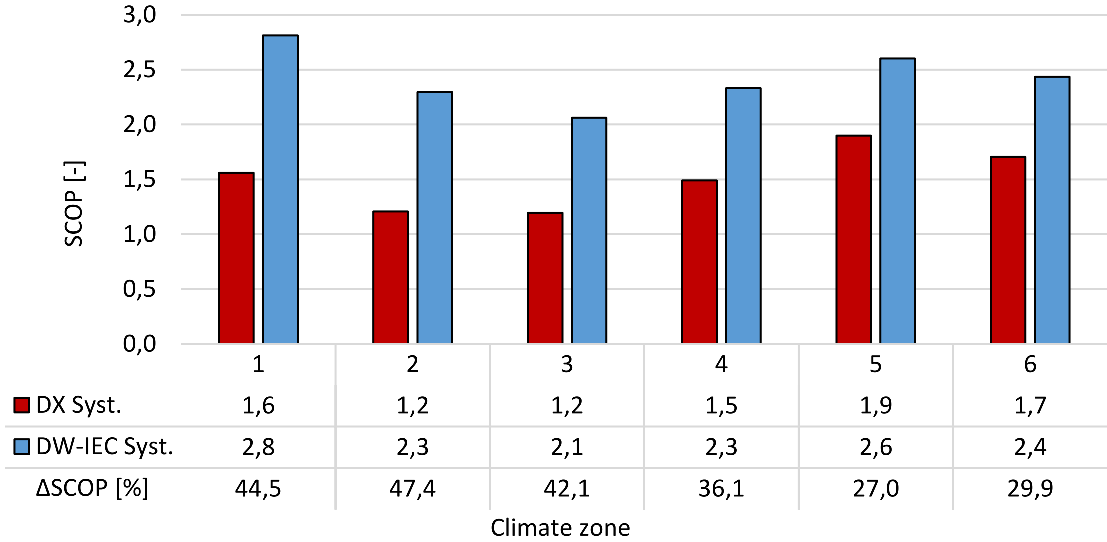

	1	2	3	4	5	6
DX Syst.	1,6	1,2	1,2	1,5	1,9	1,7
DW-IEC Syst.	2,8	2,3	2,1	2,3	2,6	2,4
ΔSCOP [%]	44,5	47,4	42,1	36,1	27,0	29,9

Fig. 12. SCOP values of the DW-IEC system and the DX system in each climate zone.

3.3.3 Energy consumption per unit of dehumidified water

The energy consumption per unit of dehumidified water, E_{cons}, was obtained for both system, in order to know the energy used only when the dehumidification demand was required. The E_{cons} results for each system and climate zone, are shown in Fig. 13. It can be observed that the lowest E_{cons} values were obtained for very hot climatic conditions, such as in climate zone 1 and the highest E_{cons} values for cool conditions, such as in climate zone 5. The trend of E_{cons} is contrary to that obtained for annual energy consumption, see Fig. 11. Comparing both systems studied, it can be observed that the E_{cons} values from the DX system were always higher than those from the DW-IEC system. The highest energy saving, ΔE_{cons}, was obtained for zone 1, 34.6 %. However, small energy savings were found for zones 5 and 6, 4.4 % and 1.7 %, respectively, climate zones with low dehumidification demand.

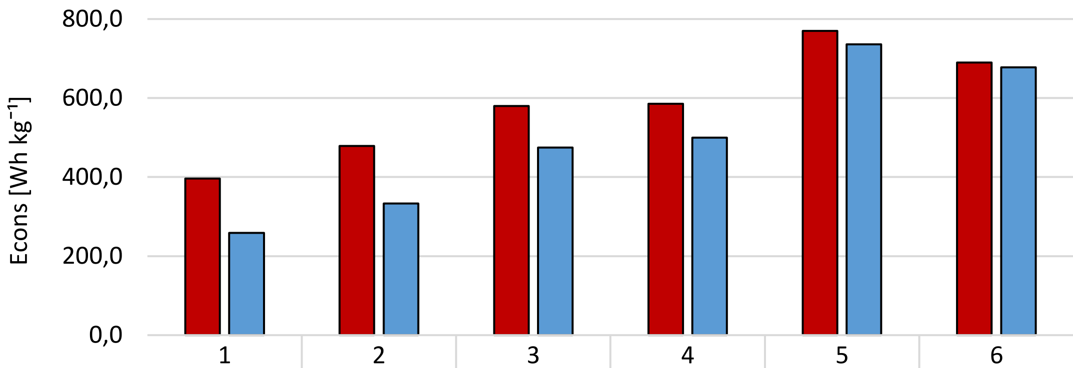

	1	2	3	4	5	6
DX Syst.	395,9	478,9	580,0	585,9	770,0	690,0
DW-IEC Syst.	259,1	332,8	474,5	500,1	736,2	678,0
ΔEcons [%]	34,6	30,5	18,2	14,6	4,4	1,7

Fig. 13. E_{cons} values of the DW-IEC system and the DX system in each climate zone.

4 Conclusions

In the present work, the energy potential and desiccant capacity of two air handling systems were analysed. The first system was composed mainly of a DW and an IEC, DW-IEC system, and the second system of a direct expansion conventional unit, DX system. Several detailed energy simulations were carried out with the assumption that both systems served a spa room. 6 different climatic conditions, from very hot zones to cold zones, were used to performed the simulations.

The results showed that the systems satisfactorily achieved the set point air conditions. Both systems delivered similar sensible and latent energy values to the building. The IEC system reduced the high air temperatures generated by the adsorption process of the DW.

The annual energy consumption of the DW-IEC system was lower than that of the DX system for the 6 climate zones, achieving significant energy savings, especially for hot climate zones with high dehumidification demand, where a 46.8 % annual energy saving was obtained. The lowest energy saving was achieved for a cool climate zone, 27.8 %. These energy savings resulted in better SCOP values for the DW-IEC system. The highest SCOP value was 2.8, obtained for a very hot climatic zone. The difference in SCOP between both systems was always greater than 25% for all climate zones.

Finally, the energy consumption per unit of dehumidified water, E_{cons}, of both systems was analysed for the 6 climate zones. Significant energy savings were obtained with the proposed DW-IEC system for very hot climate zone, due to the high dehumidification demand, achieving up to 34.6% savings. However, the energy savings of the DW-IEC system were lower for cool and cold climate zones, 4.4 % and 1.7 %, respectively, climate zones with low dehumidification demand and high heating demand.

The results suggest that the proposed system with a DW and an IEC could be a serious alternative to the DX systems composed of direct expansion units, to handle air in small buildings with high latent loads and low supply air flow rates, such as spas.

Acknowledgments

This work is related to a research stay at the Energy Department of Politecnico di Milano, Italy, and funded by the University of Cordoba, Spain.

References

[1] W.-S. Lee, C.-K. Kung, Optimization of heat pump system in indoor swimming pool using particle swarm algorithm, Appl. Therm. Eng. 28 (2008) 1647–1653. doi:10.1016/j.applthermaleng.2007.11.003.

[2] M.M. Shah, Prediction of evaporation from occupied indoor swimming pools, Energy Build. 35 (2003) 707–713. doi:10.1016/S0378-7788(02)00211-6.

[3] P. Torrero, DTIE 10.04. Covered swimming pools air-conditioned only with outdoor air, ATECYR, 2008.

[4] P. Sun, J.Y. Wu, R.Z. Wang, Y.X. Xu, Analysis of indoor environmental conditions and heat pump energy supply systems in indoor swimming pools, Energy Build. 43 (2011) 1071–1080. doi:10.1016/j.enbuild.2010.08.004.

[5] R. Tubío, N. Molero, M. Zamora, DTIE 10.06. Covered swimming pools. Systems of air conditioning, dehumidification and energy saving using heat pumps, ATECYR, 2013.

[6] L. Johansson, L. Westerlund, Energy savings in indoor swimming-pools: comparison

between different heat-recovery systems, Appl. Energy. 70 (2001) 281–303. doi:10.1016/S0306-2619(01)00043-5.

[7] J.L. Míguez Tabarés, M. Gándara Alvarez, L.M. López González, P. Fernández Viar, Feasibility study for the installation of HVAC for a spa by means of energy recovery from thermal water - Part I: Energy analysis, Renew. Energy. 23 (2001) 135–149. doi:10.1016/S0960-1481(00)00162-2.

[8] J.L. Míguez Tabarés, M. Gándara Alvarez, L.M. López González, P. Fernández Viar, Feasibility study for the installation of HVAC for a spa by means of energy recovery from thermal water - Part II: Energy analysis, Renew. Energy. 23 (2001) 135–149. doi:10.1016/S0960-1481(00)00162-2.

[9] B. Delcroix, M.A. Leduc, M. Kummert, Modeling of a portable electric spa: Model development, experimental validation and application to winter demand response, Appl. Therm. Eng. 111 (2017) 183–192. doi:10.1016/j.applthermaleng.2016.09.078.

[10] L.G. Harriman III, The dehumidification handbook, second ed., Munters Corp. Amesbury, MA. (2003).

[11] K.S. Rambhad, P. V. Walke, D.J. Tidke, Solid desiccant dehumidification and regeneration methods - A review, Renew. Sustain. Energy Rev. 59 (2016) 73–83. doi:10.1016/j.rser.2015.12.264.

[12] D.B. Jani, M. Mishra, P.K. Sahoo, Solid desiccant air conditioning - A state of the art review, Renew. Sustain. Energy Rev. 60 (2016) 1451–1469. doi:10.1016/j.rser.2016.03.031.

[13] G. Angrisani, F. Minichiello, C. Roselli, M. Sasso, Experimental analysis on the dehumidification and thermal performance of a desiccant wheel, Appl. Energy. 92 (2012) 563–572. doi:10.1016/j.apenergy.2011.11.071.

[14] F. Comino, M. Ruiz de Adana, F. Peci, Experimental study of the moisture removal capacity of a desiccant wheel activated at low and high temperature, in: CLIMA 2016 - proceedings of the 12th REHVA World Congress. Aalborg University, Department of Civil Engineering., 2016.

[15] L. Yadav, A. Yadav, Mathematical investigation of purge sector angle for clockwise and anticlockwise rotation of desiccant wheel, Appl. Therm. Eng. 93 (2016) 839–848. doi:10.1016/j.applthermaleng.2015.10.062.

[16] C.R. Ruivo, A. Carrillo-Andres, J.J. Costa, F. Dominguez-Munoz, Exponential correlations to predict the dependence of effectiveness parameters of a desiccant wheel on the airflow rates and on the rotation speed, Appl. Therm. Eng. 51 (2013) 442–450. doi:10.1016/j.applthermaleng.2012.08.037.

[17] F. Comino, M. Ruiz de Adana, Experimental and numerical analysis of desiccant wheels activated at low temperatures, Energy Build. 133 (2016) 529–540. doi:10.1016/j.enbuild.2016.10.021.

[18] C. Aprea, A. Greco, A. Maiorino, The application of a desiccant wheel to increase the energetic performances of a transcritical cycle, Energy Convers. Manag. 89 (2015) 222–230. doi:10.1016/j.enconman.2014.09.066.

[19] D.B. Jani, M. Mishra, P.K. Sahoo, Performance prediction of rotary solid desiccant dehumidifierin hybrid air-conditioning system using artificial neural network, Appl. Therm. Eng. 98 (2016) 1091–1103. doi:10.1016/j.applthermaleng.2015.12.112.

[20] J. Zhu, W. Chen, A novel multivariate linear prediction model for the marine rotary desiccant air-conditioning by adding a dynamic correction factor, Appl. Therm. Eng. 78 (2015) 101–109. doi:10.1016/j.applthermaleng.2014.12.049.

[21] Z. Duan, C. Zhan, X. Zhang, M. Mustafa, X. Zhao, B. Alimohammadisagvand, et al., Indirect evaporative cooling: Past, present and future potentials, Renew. Sustain. Energy Rev. 16 (2012) 6823–6850. doi:10.1016/j.rser.2012.07.007.

[22] B. Porumb, P. Ungureşan, L.F. Tutunaru, A. Şerban, M. BĂlan, A Review of Indirect Evaporative Cooling Technology, Energy Procedia. 85 (2016) 461–471. doi:10.1016/j.egypro.2015.12.228.

[23] A. Sohani, H. Sayyaadi, S. Hoseinpoori, Modeling and multi-objective optimization of an M-cycle cross-flow indirect evaporative cooler using the GMDH type neural network, Int. J. Refrig. 69 (2016) 186–204. doi:10.1016/j.ijrefrig.2016.05.011.

[24] M. Tu, C.Q. Ren, L.A. Zhang, J.W. Shao, Simulation and analysis of a novel liquid desiccant air-conditioning system, Appl. Therm. Eng. 29 (2009) 2417–2425. doi:10.1016/j.applthermaleng.2008.12.006.

[25] W.Z. Gao, Y.P. Cheng, A.G. Jiang, T. Liu, K. Anderson, Experimental investigation on integrated liquid desiccant e Indirect evaporative air cooling system utilizing the Maisotesenko e Cycle, Appl. Therm. Eng. 88 (2015) 288–296. doi:10.1016/j.applthermaleng.2014.08.066.

[26] H.J. Kim, S.J. Lee, S.H. Cho, J.W. Jeong, Energy benefit of a dedicated outdoor air system over a desiccant-enhanced evaporative air conditioner, Appl. Therm. Eng. 108 (2016) 804–815. doi:10.1016/j.applthermaleng.2016.07.185.

[27] P. Finocchiaro, M. Beccali, B. Nocke, Advanced solar assisted desiccant and evaporative cooling system equipped with wet heat exchangers, Sol. Energy. 86 (2012) 608–618. doi:10.1016/j.solener.2011.11.003.

[28] D. Pandelidis, S. Anisimov, W.M. Worek, P. Drag, Comparison of desiccant air conditioning systems with different indirect evaporative air coolers, Energy Convers. Manag. 117 (2016) 375–392. doi:10.1016/j.enconman.2016.02.085.

[29] M. Goldsworthy, S. White, Optimisation of a desiccant cooling system design with indirect evaporative cooler, Int. J. Refrig. 34 (2011) 148–158. doi:10.1016/j.ijrefrig.2010.07.005.

[30] E. Elgendy, A. Mostafa, M. Fatouh, Performance enhancement of a desiccant evaporative cooling system using direct/indirect evaporative cooler, Int. J. Refrig. 51 (2015) 77–87. doi:10.1016/j.ijrefrig.2014.12.009.

[31] J.D. Chung, D.Y. Lee, Contributions of system components and operating conditions to the performance of desiccant cooling systems, Int. J. Refrig. 34 (2011) 922–927. doi:10.1016/j.ijrefrig.2011.03.003.

[32] S.D. White, P. Kohlenbach, C. Bongs, Indoor temperature variations resulting from solar desiccant cooling in a building without thermal backup, Int. J. Refrig. 32 (2009) 695–704. doi:10.1016/j.ijrefrig.2009.01.019.

[33] CIAT, http://www.grupociat.es/, (accessed 05.07.17).

[34] Klein, S.A. 2006. TRNSYS 17: A Transient System Simulation Program, SEL, University of Wisconsin, Madison USA.

[35] RITE 2007. Reglamento de instalaciones térmicas en los edificios, Real Decreto. (2007) 35931–35984.

[36] F. Comino, S. Milani, S. De Antonellis, C.M. Joppolo, M. Ruiz de Adana, Indirect evaporative coolers: development of a simplified correlation and comparison with a phenomenological model and experimental data, Energy Build, submitted to the journal.

[37] F. Comino, A. Cerezuela, M. Ruiz de Adana, M. Zamora, F. Peci, Numerical study of hybrid HVAC systems with desiccant wheel, in: V Ibero-American Congress of sciences and techniques of the cold., Tarragona, Spain, 2014: pp. 433–443.

[38] SODECA, http://www.sodeca.es/, (accessed 05.07.17).

[39] ASHRAE STANDARD 90.1 Energy Standard for Buildings Except Low-Rise Residential Buildings, Society. 8400 (2007) 404–636. doi:http://dx.doi.org/10.1108/17506200710779521.

[40] Meteotest (2003). Meteonorm handbook, Parts I, II and III. Meteotest, Bern, Switzerland. http://www.meteotest.ch, (accessed 05.07.17).